Advances in tailoring the water content in porous carbon aerogels using RT-pulsed fluorination

Yasser Ahmad, Sandrine Berthon-Fabry, Marian Chatenet, Guillaume Monier, Marc François Pierre Dubois, Katia Guérin

Version of Record: https://www.sciencedirect.com/science/article/pii/S0022113920303316
Manuscript_d92eb830976c54accf2ac3070f34119d

Advances in tailoring the water content in porous carbon aerogels using RT-Pulsed fluorination

Yasser Ahmad[1, 2*], Sandrine Berthon-Fabry[3], Marian Chatenet[4], Guillaume Monier[5], Marc Dubois[1], Katia Guerin[1]

[1] Université Clermont Auvergne, CNRS, SIGMA Clermont, ICCF, F-63000 CLERMONT-FERRAND, FRANCE
[2] Fahad Bin Sultan University, P. O Box 15700, Tabuk, 71454, Kingdom of Saudi Arabia
[3] MINES ParisTech, PSL University, PERSEE - Centre procédés, énergies renouvelables et systèmes énergétiques, CS 10207 rue Claude Daunesse 06904 Sophia Antipolis Cedex, France
[4] Univ. Grenoble Alpes, CNRS, Grenoble INP (Institute of Engineering Univ. Grenoble Alpes) LEPMI, 38000, Grenoble, France
[5] Université Clermont Auvergne, CNRS, SIGMA Clermont, Institut Pascal, F-63000 CLERMONT-FERRAND, FRANCE
Corresponding author * Yasser Ahmad: e-mail: yahmad@fbsu.edu.sa, Mobile: +966532334641.

Abstract

The present work introduces a safe and efficient fluorination method, called RT-pulsed fluorination, proceeding under pure fluorine gas. The RT-pulsed fluorination enables to modify the surface chemistry of carbon aerogels (CAs), materials which suffer from water trapping into their porosity and their low degree of graphitization, hence limiting their application. This new fluorination route was developed to reach several goals, such as preventing the generation of structural defects, maintaining the tailored porous texture of the aerogel, favoring covalent C-F bonding without promoting CF_2 and CF_3 groups, and repulsing the water trapping into the porosity. The impact of the RT-pulsed fluorination on the conductivity will be also discussed.

Highlights

- Carbon aerogels hold great technological promise for a variety of sustainable energy applications.
- Carbon aerogels suffer from water trapping into their porosity, which can severely handicap the intended process.
- RT-pulsed fluorination is a safe and efficient method to modify the surface chemistry of carbon aerogels.
- Fluorination is an efficient way to tailor the amount of water in porous carbon.

Keywords: RT-pulsed fluorination, surface chemistry, carbon aerogels, water trapping

Graphical abstract

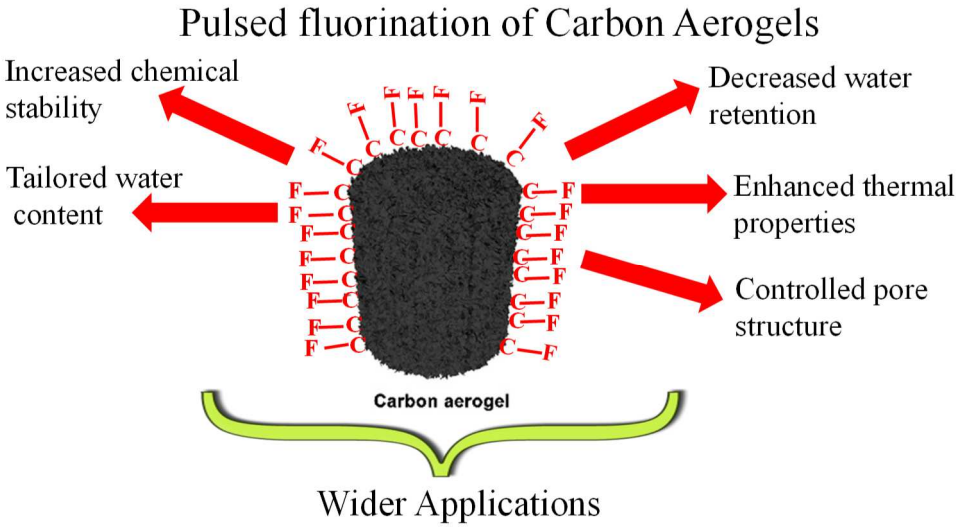

Introduction

Just like the other interesting forms of carbon-based nanomaterials such as zero-dimensional buckyballs, one-dimensional carbon nanotubes (CNTs), and the relatively new class of two-dimensional graphene nanosheets, porous carbons are another important class of carbon nanomaterials. The development of these three-dimensional nanoporous carbons holds great technological promise for a variety of sustainable energy applications, including energy storage, adsorption and catalysis, sorbents, and desalination [1-7]. The utility of porous carbons is derived from their high surface area, three-dimensional structure, chemical stability, the abundance of carbon, and their low mass density[8].

Despite their fascinating properties and applications, the presence of water in the graphitic porosity of CAs can severely handicap the intended process. For example, quite low humidity in gases entering industrial adsorbers are known to have a large effect on the capacity and selectivity for the removal of organic and inorganic contaminants [9]. Similarly, small amounts of water often reduce the diffusion rates of alkanes in microporous media by an order of magnitude [7, 10]. Also, the presence of water in activated carbons has a large effect on the performance of industrial adsorbers, often reducing their useful lifetime by as much as 50% [7].

So, developing a method that gives scientists the ability to tailor the amount of water in porous carbon as well as other physical properties would without a doubt enhance the potential utility of this class of carbon nanomaterials. Fluorination is a perfect way to increase the hydrophobicity of materials [11]. The key to the impact of fluorination is the decrease in affinity for water by the conversion of hydroxyl groups into C-F bonds [11]. Besides, the pore structure of the material, which is of paramount importance in some applications such as fluid separation and gas storage applications, can be controlled through careful adjustment of fluorination conditions.

In the last few decades, numerous studies have been devoted to the fluorination of graphite or graphitized carbons such as fullerenes C(60), carbon nanotubes (CNTs), carbon blacks, and many others [12-17] and to the characterization of the fluorinated compounds, which have found important practical applications.

In this work the fluorination of an interesting class of porous carbon, in particular, carbon aerogels (CAs) is reported. Carbon aerogels, owing to their tailored porous structure, are materials of choice to design media compatible with mass-transfer, this has recently led to multiple studies aiming at using CA in electrocatalysis, notably as fuel cell electrodes [18, 19]. One of the drawback of CA for electrochemical applications, though, is their intrinsic non-graphitized structure, which is not compatible with long-term durability in operation (the

cathode in fuel cells operate in highly oxidizing conditions [20, 21]. This issue can be mitigated by "protecting" the carbon surface via appropriate surface treatments, e.g. metal-oxides deposition [22] or fluorination [23]. Fluorination may have other advantageous effects regarding the physicochemical properties of the CA support, though.

Tailoring the water content and/or trapping in the porosity of CAs and thus make the surface of these materials hydrophobic, (i.e. water-repelling), as well as improving the uniformity, and key properties of the material is also mandatory in many practical applications. To the best of our knowledge, there are very few experimental techniques in the literature that aim to tailor the water content within porous materials, and this originates from the difficulty to prepare well-characterized carbon structures. Gaining a comprehensive understanding by experiment alone has not been successful thus far. For instance, Brennan et al. used experimental investigations, semi-empirical approaches, and simulation studies that offer the possibility of studying many phenomena exclusively and systematically for precisely defined model materials [7].

The functionalization of these carbon aerogels via surface engineering has led to a host of interesting composite aerogels that could make CAs promising candidates for an even wider array of applications.

The high reactivity, oxidizing properties, and the highest electronegativity of fluorine offer the ability to create very strong bonds with the majority of other elements. Therefore, fluorine compounds provide a unique tool to modify the surface properties of materials [24-26]. In particular, fluorination is one of the methods enabling an efficient functionalization of carbonaceous materials. The C-F bonds and the atomic F/C ratios deeply depend on the nature of the raw carbon materials, their sp^2 ratio, their structure, and fluorination conditions (temperature, reaction duration, pressure, composition of the gaseous reactants, in particular the presence of HF or fluorides besides F_2 which may act as catalysts) [27-31]. Thus, the key point of fluorinated carbon materials is mainly about the design of carbon materials and the optimization of fluorination conditions [29, 32-37].

The C-F bonds are formed based on the fluorination reactions between carbon materials and fluorinating agents. Because the F atom has extremely high electronegativity, fluorinated carbon involves various C-F bonding characteristics of ionic, semi-ionic, and covalent bonds [38-40]. Besides, based on theoretical calculation, the C-F bonds depend on the fluorination levels (F/C ratios) [27]. If the fluorination conditions are not well set, F/C atomic ratio higher than 1 can be obtained and lead to either solid CF_2 and CF_3 groups or volatile species such as CF_4 or C_2F_6. Depending on the fluorination mechanism, different kinds of bonding can occur

and when hyperfluorination occurs and forms gaseous species, it implies carbon extraction and huge degradation of the structure and texture of carbon [41, 42]. Thus, optimizing the composition of C-F bonds and F/C ratios is an efficient approach to obtain tailored fluorinated carbon. Up to now, great progress has been achieved in the research of fluorinated carbon, especially regarding the fluorination method used.

Various fluorination methods can be applied to modify the intrinsic properties of materials. The synthesis methods of fluorinated carbon (denoted CFx) can be mainly classified into direct gas fluorination, indirect fluorination [43] during which a hydrocarbon substrate reacts *in situ* with free radicals of fluorine, plasma-assisted fluorination [12– 14], controlled fluorination using fluorinating agents (such as terbium tetrafluoride TbF_4 and xenon difluoride XeF_2) [12, 44-47], and anhydrous hydrogen fluoride (HF) [48]. Due to its high toxicity, reactivity, and corrosiveness, fluorination using HF is of limited scope [49] and will be disregarded hereafter.

Direct fluorination (also called dynamic fluorination, DF) using a continuous flow of pure fluorine gas F_2 remains the most known and useful method to obtain fluorinated carbon materials, thanks to the high reactivity of molecular fluorine. Despite its importance, direct fluorination could have a lot of disadvantages in some particular cases, especially when it comes to fluorinate highly porous materials: indeed it may lead to the collapse of the porosity of the carbon structure. Moreover, direct fluorination is not suitable when a F/C fluorine content lower than one ($F/C < 1$) is required, or when the starting material exhibits high specific surface area and a high sp^3 hybridized carbon amount, such as carbon aerogels (CAs).

Controlled fluorination is particularly useful as the thermal decomposition of the fluorinating agents produces atomic F and/or molecular F_2. This makes it possible to progressively release a definite quantity of reactant upon the fluorination duration and thus to control both the reactivity with fluorine and the fluorine level [16, 17, 50, 51]. As an illustration, controlled fluorination using the thermal decomposition of XeF_2 fluorinating agent (reported elsewhere [52, 53]), has enabled an efficient functionalization of carbon aerogels and made fluorinated CA more resistant to the corrosion phenomenon that occurs in proton exchange membrane fuel cells or batteries; in particular, longer life of the battery was achieved [12, 18, 23, 52, 54, 55]. Also, Zhang et al. [46] and Ahmad et al. [47] have fluorinated carbon nanofibers and carbon nanodiscs, respectively, using the thermal decomposition of TbF_4 that released mainly atomic fluorine F• [44]. The resulting CFx were used in primary lithium batteries and led to increased electrochemical performances [47, 56]. However, this controlled fluorination method has a high cost compared to traditional fluorination methods using molecular fluorine. Also, the process should be conducted in a closed reactor in the temperature from 420 to

500°C; these fluorination conditions are too harsh to be applied to carbon aerogels, as they may lead to destruction of the materials' porosity.

The present work provides a direction for tuning C-F bonding and F/C ratios, developing a safe and efficient fluorination method. This method, the so-called "RT-pulsed fluorination" (RT stands for room temperature), allows to optimize the fluorination conditions during the preparation of fluorinated carbon aerogels. It is designed simple enough to enable its future popularization and usage of the obtained functional materials in numerous practical applications. More specifically, the contribution will precisely detail the fluorination procedure of CAs using the RT-pulsed fluorination; an overview of the obtained materials' final properties, as well as potential sources of performance improvement of the process, will also be described.

2. Experimental

2.1. Synthesis

2.1.1 Carbon aerogel synthesis

The synthesis protocol of the Carbon Aerogels was inspired by the Pekala method [57] and is described in earlier contribution [23].

2.1.2 Fluorination and chemical composition of fluorinated samples

Gaseous fluorine was purchased from Solvay Fluor (purity 98–99% v/v with HF max. 0.5% v/v and other gases, primarily O_2 /N_2 at approximately 0.5% v/v).

Fluorinated carbon aerogels were prepared using the dynamic and pulsed fluorination operating at room temperature. Whatever the fluorination route, a Monel reactor and a Ni boat, which had been previously both passivated (covered with NiF_2) were used. Before each fluorination, samples were outgassed overnight at 120°C under primary vacuum to eliminate adsorbed molecules from their surface or engaged in their porosity. This is particularly important for adsorbed water, whose presence at the surface of the samples would lead to the formation of HF, resulting in inhomogeneous fluorination.

After fluorination, the reactor was purged with nitrogen to replace the residual molecular fluorine and possible decomposition products like NF_3, CF_4, and C_2F_6. Finally, all samples were outgassed at 150°C for 2 hours under primary vacuum, to eliminate the weakest C-F bonds and adsorbed molecules like F_2, HF, NF_3, and C_2F_6. All the fluorinated samples are labeled: CA-fluorination method-CFx, as shown in Table 1.

The fluorination conditions for the methods were set with the common aim that fluorinated materials prepared to obtain a target chemical composition of $CF_{0.25}$ for the fluorinated materials. This fluorine level is fair enough for the possible applications of CA cited in this work.

For each aerogel prepared, the fluorination level '*x*' in CF*x* composition, i.e. F/C atomic level, of fluorinated carbon aerogels was determined by gravimetry upon fluorination (weight uptake), and X-ray photoelectron spectroscopy (XPS). Table 1 shows the data of all fluorinated samples.

2.1.3 Fluorination Procedure

Whatever the fluorination method, and because of F_2 high reactivity, the fluorination conditions (i.e time of reaction, temperature, nature of fluorinating agent, rate of fluorine addition…), depending on the intrinsic properties of the carbon used (graphitization degree, morphology, shape, texture, porosity…) should be carefully controlled to avoid any decomposition of the carbonaceous matrix [58]. The "RT-pulsed fluorination" described herein is quite similar to that of static fluorination, but does not exhibits its drawbacks. The common point between the two methods (i.e static and pulsed) is to introduce a pre-calculated quantity of F_2 upon the fluorination duration and the mass of carbon to fluorinate and thus to control both the reactivity with fluorine and the fluorine level. The main difference between static and pulsed fluorination is that during the static method the desired amount of F_2 gas is introduced as a whole into the reactor, i.e progressive one-shot introduction of F_2 gas. On the contrary, for the pulsed fluorination, the desired quantity of F_2 gas is introduced slowly in the form of very small injections. For instance, if we suppose that the desired amount of F_2 gas that should be introduced into the reactor is X, the injection of X is done in *n* times, i.e each injection has an amount of X/*n* of F_2, where *n* depends on the fluorination conditions i.e the initial mass of C, its porosity, and the fluorination temperature. The small F_2 injections allow to observe at real-time the phenomenon of absorption of the introduced quantity of F_2 with a highly porous and reactive carbon matrix like the carbon aerogels used in this work (Figure 1). In other terms, the reaction between F_2 and CA is perfectly controllable in terms of the reacting quantity of F_2, and more importantly to discern when the F_2-CA reaction begins and when it ends. This is important because it highlights the low synthesis cost of this method, since the amount of F_2 used to fluorinate is perfectly controlled (unlike the dynamic fluorination that operates under a flux of F_2) and it avoids any decomposition phenomenon of the carbon into volatile species such CF_4 and C_2F_6 [33, 59, 60], as this method operates at room temperature. The fluorination modifies the texture of the CAs by increasing the pore

size and decreasing the specific surface area, but the textures remain appropriate for proton exchange membrane fuel cell (PEMFC) applications as it was shown in recent studies [22, 55]. The fluorination parameters were set in order to limit the fluorine atom per carbon atom to 0.25 (i.e $CF_{0.25}$) and to avoid any decomposition process of carbon into gaseous fluorinated carbons like CF_4 and C_2F_6 [32, 33].

2.1.4 Physico-chemical characterizations

Chemical composition

X-ray photoelectron spectroscopy (XPS) measurements were performed in an ultrahigh vacuum photoelectron spectrometer equipped with an Omicron DAR 400 X-ray source and an Omicron EA 125 hemispherical analyzer. The Mg Kα source (1253.6 eV) running at 300 W is separated from the analyzer by an angle of 55°. A high magnification mode and constant pass energy of the analyzer equal to 20 eV were used for analysis. Photoelectron data were recorded at a take-off angle of 90° (normal detection). High resolution spectra were recorded with an energy step of 0.1 eV. The electron binding energies were corrected according to the usual energy referencing to the C-C and C-H bonds at 284.3 eV. Binding energies, line widths and areas of the different XPS peaks were obtained by a weighted least-squares fitting of a Lorentzian-Gaussian model curve to the experimental data using the program XPSPEAK41. The atomic percentages were obtained using the empirical formula of XPS signal intensity [61] considering a homogeneous atomic concentration and the accurate spectrometer calibration described in reference [62].

Structural characterizations

NMR experiments were performed at room temperature using a Bruker Avance spectrometer, with working frequencies for ^{13}C and ^{19}F of 73.4 and 282.2 MHz, respectively. A Magic Angle Spinning MAS probe (Bruker) operating with 2.5 mm rotors was used. For MAS spectra, a simple sequence was performed with a single $\pi/2$ pulse length of 4.0 and 3.5 µs for ^{19}F and ^{13}C, respectively.^{13}C chemical shifts were externally referenced to tetramethylsilane (TMS).^{19}F chemical shifts were referenced with respect to CF_3COOH.

Raman spectroscopy was used to study the structure of the different carbon materials. The spectra were recorded *ex-situ* using a Jobin Yvon T64000 spectrometer. The wavelength LASER excitation was equal to 514 nm. Each sample was analyzed in five different areas and the final curve is the average of the five measurements. For the sake of comparison, the Raman spectra were normalized to the intensity of the graphitic lattice band ($\nu \approx 1585$ cm^{-1}). For the carbon materials, three main bands could be detected [4]. That is why spectra were

recorded in intervals including these Raman shifts. The lateral extension of the graphite planes (hereafter denoted by L_a) was determined with the Knight and White formula: "L_a = 4,4 * (A_{Gband}/A_{D1band})" [63], where A_G band and A_{D1}band are respectively the areas of the G and D1 band. The G and D2 bands are close ($\nu \approx 1585$ cm^{-1} and $\nu \approx 1610$ cm^{-1} respectively), so curve fitting was performed using LabSpec software to calculate precisely the area of the G band.

Textural characterization

The various samples were characterized by **Transmission Electron Microscopy** using TEM 2010 Jeol, with LaB_6 filament and a resolution of 0.19 Angstrom operating at 200 kV. The nanomaterials were dispersed in ethanol using an ultrasonic bath. Few drops of the suspension were deposited onto a copper support grid covered with an ultrathin carbon/formvar films. The grids were subsequently dried at ambient conditions before the introduction in the TEM.

Morphologies of the different carbons were also analyzed by **Scanning Electronic Microscopy** (SEM) using a Cambridge Scan 360 SEM operating at 3.00 kV.

Electrical conductivity

The electrical conductivity was investigated by a direct resistance measurement at room temperature with a home-made cell. 50 mg of powder was introduced between two copper electrodes (surface equal to 0.7854 cm²) surrounded by a Teflon ring. Different currents were applied (-105 mA, 105 mA and 400 mA) thanks to a potentiostat (Biologic HPC-803) without applying pressure (mass applied 0) or at a pressure equal to 6.37.10^7 Pa (mass applied (0.5 t). The value of the tension for each current was recorded. The electrical conductivity values (σ) were calculated as an average of the 3 values obtained with the 3 currents using the formula: "$\sigma = e.I/U.S$", where e is the thickness of the sample (cm), I the current applied (A), U the tension recorded (V) and S the surface of the electrode (cm^2).

Thermal properties

TGA experiments were carried out in air on Shimadzu TGA-50. The heating rate is of 2°C.min^{-1} going from room temperature to 600°C. The mass of the sample analyzed is about 20 mg ±0.001 mg. Both samples were analyzed using the same conditions. for a detailed thermal study, many parameters could be extracted from the TGA curves and their derivatives: (i) T_{10} (extracted from the curves) is the temperature corresponding to 10% weight loss, (ii) T_{C-F}, (from the derivative TGA curve), which is the decomposition temperature of the carbon-fluorine C-F bond (defluorination mechanism) and (iii) T_C (from

the derivative TGA curve), which represents the decomposition (i.e burning in air) temperature of the (non-fluorinated) carbon. In this paper, we will show the T_{C-F} parameter that gives an idea of the thermal stability of the C-F bond within the fluorinated samples.

3. Results and discussion

3.1 Fluorination mechanism and choice of fluorinated aerogels.

Thus dynamic and pulsed fluorinations were performed and led to about same chemical composition of atomic ratio F/C equals to 0.25 i.e. $CF_{0.25}$ for the fluorinated carbon aerogels.

- For the dynamic process, 100 mg of CA were placed under a pure fluorine gas flow at atmospheric pressure and room temperature; the resulting sample is denoted CA-DF-CFx (DF for Dynamic Fluorination, *x* is the F/C at. ratio in the sample).

  This direct fluorination proceeds with an excess of molecular fluorine, leading to low reaction yield. The major drawback of the direct fluorination that operates under a continuous flow of non-diluted F_2 gas, is that it is not scalable i.e. the synthesis of CFx cannot be carried out at a large scale because it may lead to non-homogenous fluorination and the exfoliation of the carbonaceous material because of the large amount of fluorine gas used. Furthermore, the fluorination reaction being exothermic, it would result in the degradation of the carbon aerogel because of the local increase of the temperature.
- For pulsed fluorination (PF), pure molecular fluorine gas is introduced in a closed reactor through small and successive additions. The introduced quantity reacts with the CA inside the reactor. This fluorination method allows the synthesis of larger amounts of fluorinated CAs (around 2 g) while for the dynamic mode, around 100 mg of CA were fluorinated. This is a favorable point for the PF that allows an upscaling i.e. the synthesis of larger quantities of CFx to industrial levels is doable with the PF method. In any case, the pulsed fluorination allows to fluorinate larger amounts of carbon aerogels while keeping homogeneous fluorination i.e. the good distribution of fluorine atoms in the carbon matrix.

It is to be noted that the carbon aerogels used in this work are highly reactive towards fluorine gas because of its low graphitization degree. Thus the fluorination temperature (T_F) can be decreased to room temperature. Each successive amount of F_2 introduced is fixed by the measurements of both the temperature and the pressure in the reactor. Low pressure change evidences the completion of the equilibrium and another addition can be done. In such

operating conditions, the number of injections defines the desired fluorination rate. The amount of fluorine to introduce into the reactor at Standard Pressure and Temperature (STP) to react with the CA must be pre-calculated before the fluorination. For this, we used the ideal gas equation of state ($PV = nRT$), taking in consideration the initial mass of carbon to fluorinate, the temperature inside the reactor (room temperature i.e 25°C), the volume of the reactor in which the fluorination takes place: V = 950 mL, and the atmospheric pressure (1 bar). This leads to the number of moles (n) of F_2 and thus the mass of fluorine to be introduced considering the molar mass of difluorine ($M(F_2)$ = 38 g/mol).

The amount of fluorine introduced is previously calculated according to the mass of carbon to fluorinate. The resulting sample is denoted CA-PF-CFx (PF for Pulsed Fluorination, x is the F/C at. ratio in the sample).

The reactivity of fluorine with the carbon aerogels is shown in Figure 1; it proceeds in 4 steps, as summarized below:

- Step 1. Vacuum: A primary vacuum is applied to the reactor to evacuate humid air and to remove completely any impurity that could compromise the fluorination procedure. The vacuum is applied for at least 2 h for each sample. When the pressure is stabilized inside the reactor, fluorine is gradually introduced into the reactor.
- Step 2. Prompt reaction kinetics: as soon as fluorine is introduced into the reactor (first injection), it rapidly reacts with the CA, resulting in the steep consumption slope in Figure 1. During the first F_2 injection, 2 phenomena may happen: the first one is a purification of the carbon lattice because of the high reactive and oxidative character of fluorine gas. F_2 initially reacts with all the surface impurities and/or groups of the carbon within the pristine sample. After that, fluorine grafting begins on the surface vacant sites of the carbon.
- Step 3. Reaction kinetics slow down: after several F_2 injections and relatively intense conversion with the carbon, the amount of fluorine introduced would take a little longer to react with the CA. The latter have already fixed a certain amount of fluorine and the vacant sites for the fixation of fluorine are becoming increasingly rare.
- Step 4. Fluorination almost stops: the theoretical quantity of fluorine pulses was gradually introduced until the reaction (i.e. the consumption of F_2) becomes very slow or even stops. Once all surface vacant sites are bonded with fluorine atoms,

the introduced F_2 gas will remain in the reactor without reacting with the carbon. This can be visible by the drastic change in pressure inside the reactor: the pressure remains nearly constant long after the introduction of F_2 meaning that the aerogels are, at this stage, saturated with fluorine. Grafting fluorine on the carbon matrix becomes more and more difficult as that can be explained by the decreasing number of fluorine binding sites present in the sample. At this time, the kinetics of the reaction between carbon aerogels and F_2 gas becomes very slow at the pressure and temperature conditions used during the fluorination.

The flux of fluorine gas is generally between 1 and 50 $mL.min^{-1}$ on levels ranging from 5 to 60 min (Figure 1). The calculated additions provide the exact reactive quantity of F_2 to obtain a composition up to 0.25 (i.e. $CF_{0.25}$). All syntheses were made successfully with a reaction yield close to 95%.

The atomic ratio determined by weight gain is F/C = 0.25 after synthesis for total contact time with fluorine of about 70 min.

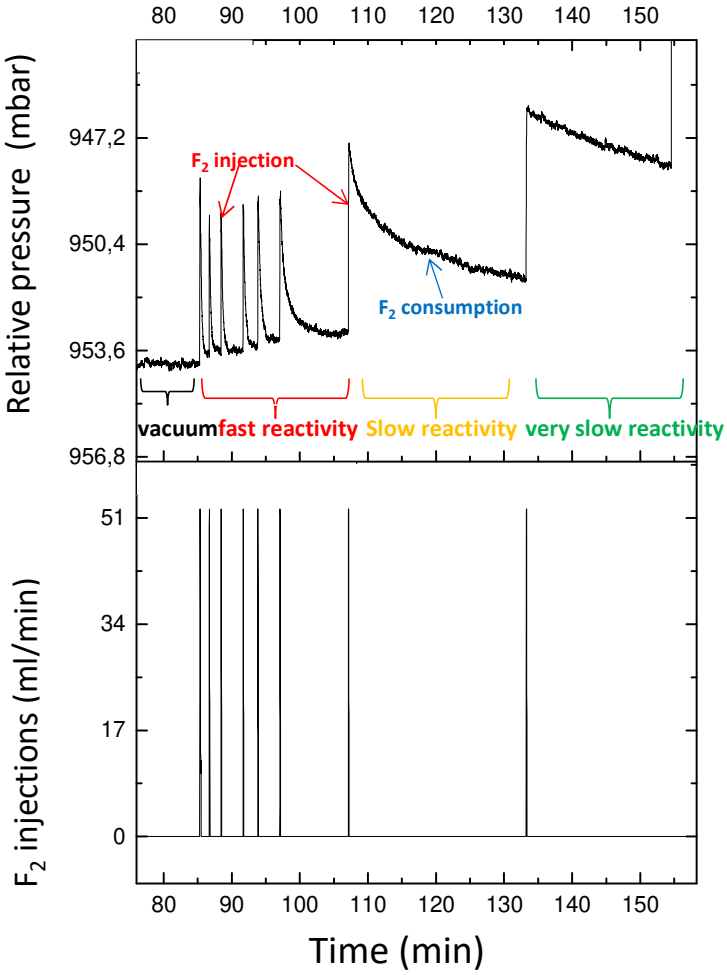

Figure 1. Relative Pressure P (mbar) and fluorine injections (ml/min) data during pulsed fluorination of carbon aerogel operating at room temperature

Table 1. Fluorination operating conditions and estimated F/C ratio for each sample

Fluorination method	F/C (weight uptake)	Procedure	Fluorination temperature, T_F (°C)	Fluorination duration (min)	CFx reference
Dynamic	0.26	Excess of F_2 (continuous flow of F_2)	Room temperature	180	CA-DF-$CF_{0.26}$
Pulsed	0.25	Injections (exact quantity of reactive F_2)	Room temperature	70	CA-PF-$CF_{0.25}$

In terms of their parameters, dynamic and pulsed fluorinations operate both at room temperature as shown in Table 1 (T_F = RT). However, the other operating parameters (time of reaction and quantity of F_2) seem to be better for pulsed fluorination compared to dynamic one. In particular, as we mentioned earlier, the amount of reactive fluorine F_2 is a predefined and accurate quantity for PF, while a large excess of F_2 for the DF as it operates under a continuous flow. With that said, the PF technique clearly has a reduced cost for producing fluorinated aerogels in terms of quantity of fluorine used as well as reaction time (70 and 180 min for PF and DF, respectively). Thus, the PF technique is most likely to suit production of fluorinated aerogels at larger scale than the DF method.

In what follows, we will discuss the physico-chemical characteristics of fluorinated CAs prepared using pulsed fluorination (named CA-PF-$CF_{0.25}$) and direct fluorination (CA-DF-$CA_{0.26}$) in order to define the most suitable approach to fluorinate this type of porous carbonaceous materials and to open the door of their application and industrialization.

3.2. Textural characteristics

Figure 2 shows the texture of the pristine CA using SEM and TEM techniques. The CAs are macroporous open cell foams that consists of carbon nanoparticles bonded to each other leading to a textured material with open porosity. The diameter of these nanoparticles is estimated between 15 nm and 18 nm from TEM and SEM images, respectively, as calculated from the particle size distribution histograms (Figure 2). XPS and EDX measurements revealed mainly the presence of the carbon element in the matrix (95% C) and the rest is O.

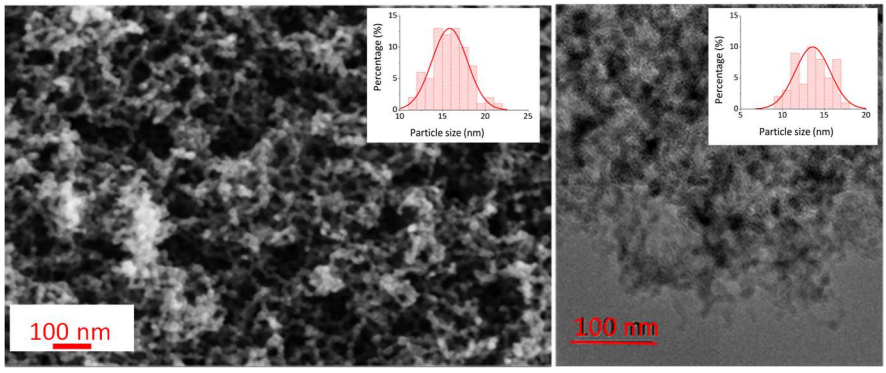

Figure 2. SEM (on the left) and TEM (on the right) images and histograms of particle size distribution for the pristine carbon aerogels.

After fluorination, the morphology of the fluorinated samples obtained by pulsed and dynamic fluorination is quite similar as it is attested in Figure 3 that shows the TEM micrographs of the fluorinated samples. The histograms reveal a decrease of particle size

which can be seen as a de-agglomeration of the raw sample. Indeed, the TEM histogram before fluorination reveals in fact two particle size distributions: one around 10-12 nm and another at higher size (16-17 nm), which can be associated to the packing of particle size. Fluorination allows to separate some particles, this process being more efficient for pulsed fluorination than for direct fluorination. It must be noted right now that those packing can favor water trapping. The X-EDS analysis indicates a fluorination rate of between 0.25 and 1.75 at.% for both samples depending on the zones analyzed. This ratio is rather low, because of (i) the presence of carbon from the TEM grid (the conductive membrane substrate) which adds to the carbon from the sample, leading to overestimation of the carbon content in the sample (hence underestimation of its F content) and (ii) the possible release of volatile F-containing species under the electron beam. The apparent structure of the fluorinated aerogel does not differ from the pristine sample (see Figure 2).

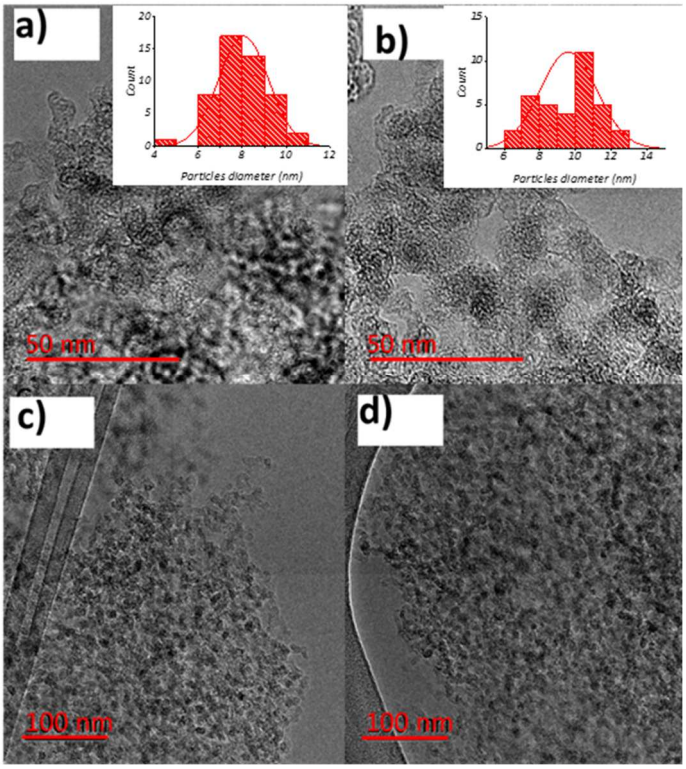

Figure 3. TEM images and histograms of CA-DF-$CF_{0.26}$ (a,c) and CA-PF-$CF_{0.25}$ (b,d)

3.3 Raman spectroscopy

The Raman spectra of the initial aerogels the samples are displayed in Figure 4. The spectra were recorded in at least 5 different areas of the samples. No difference was found whatever the location which shows the homogeneity of the sample. The spectra were normalized to the intensity of the G band. Two narrow vibration bands with a full width at half maximum of about 20 - 40 cm^{-1} are visible. The Raman's shifts around 1356 and 1589 cm^{-1} are assigned to

the D and to the conventional G mode, respectively. This last mode is related to the graphitization degree of carbon material and is also called tangential mode (where the carbon atoms in sp^2 hybridization vibrate parallel to the axis of the nanotube) [64]. The D band has a high intensity for the starting aerogels indicating a low degree of order. By deconvoluting the spectrum by Lorentzian components, an I_D / I_G ratio of 1.55 are found reflecting an high rate of structural disorder in the aerogels.

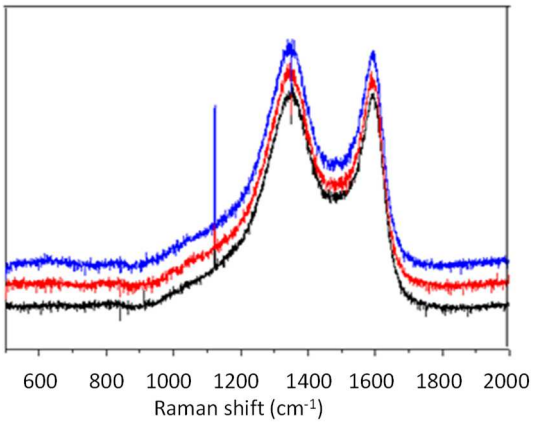

Figure 4. Representative Raman spectra of pristine carbon aerogels for three different zones.

The Raman spectra of the different fluorinated samples are shown in Figure 5. For each fluorinated sample, at least 5 regions were scanned within the sample, we can see that the spectra at different regions are perfectly superimposable which shows the homogeneity of fluorination among the samples. When deconvoluting the spectrum by Lorentzian components, I_D/I_G ratio of 1.55 is found whatever the fluorination method, i.e. similar to the starting material. Already disordered in the precursor, the carbon structure is not changed during the fluorination. In other words, fluorination does not bring additional disorder to the CA sample.

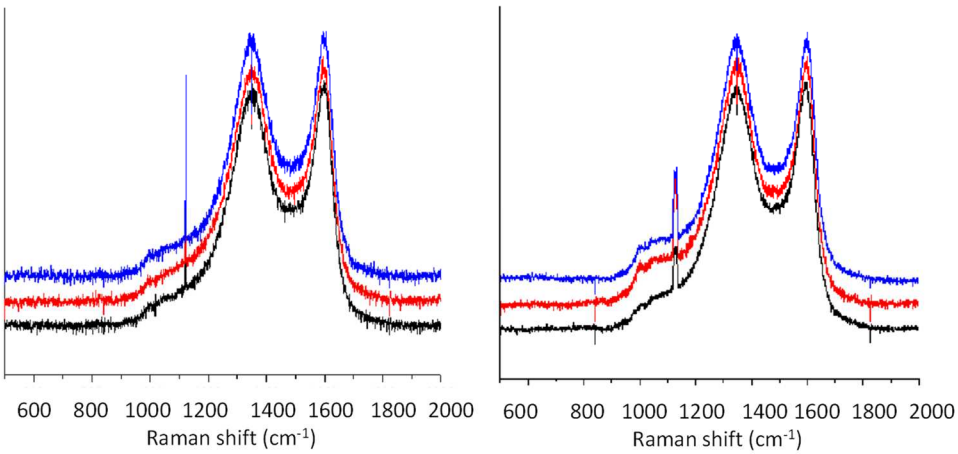

Figure 5. Raman spectra of fluorinated for 3 different regions of the fluorinated carbon aerogels using 2 fluorination methods: CA-PF-$CF_{0.25}$ on the left, and CA-DF-$CF_{0.26}$ on the right.

3.4 NMR spectroscopy

NMR is a powerful tool to investigate the carbon-fluorine bonding [42, 65-67]. So ^{19}F and ^{13}C MAS NMR operating at spinning rates of 34 and 10 kHz, respectively, were carried out. The spectra are shown in Figure 6 (a) and (b) respectively. The expected chemical shifts for the covalent C-F bonds are between -140 and -190 ppm / $CFCl_3$ [65-69]. The higher the covalence, the lower the chemical shift. The presence of non-fluorinated carbons near C-F results in hyperconjugation and a weakening of the C-F bonding [70, 71]. In other words, the lower the fluorine density is (around a C–F bound), the higher the ^{19}F chemical shift is.

The chemical shifts of the CF_2 and CF_3 groups appear around -120 and -80 ppm, respectively. The magic angle spinning procedure allows chemical displacement anisotropy to be suppressed and ^{19}F-^{19}F homonuclear dipolar coupling to be decreased. The different lines are then usually well separated for fluorinated graphitized carbons [70, 71].

A very few amount of CF_3 groups is evidenced by ^{19}F data regarding the line at -80 ppm. The broad line in a range from -143 to -195 ppm is assigned to C-F bonds and fluorine in interaction with the fluorocarbon lattice. Nevertheless, a line at -120 ppm related to CF_2 groups cannot be excluded. Anyway, when a decomposition occurs during fluorination of porous carbons, this line exhibits a high intensity [72]. The present data evidence no or very low decomposition during fluorination.

Two different lines are observed for C-F bonds: i) a broad one that results from the overlapping of different components related to C-F with different neighboring (spinning rate of 34 kHz cannot decrease the linewidth). One type of Carbon/Fluorine interaction is favored and a narrow line appears on the spectra at - 180 ppm. This line has been reported for other fluorinated porous carbons [73, 74]; an annealing at 150 °C for 2 h under primary vacuum resulted in a decrease of this particular component and it disappeared almost totally when the temperature or duration was increased. It was assigned to an intermediate stage involving labile fluorine atoms like fluorine–Graphite Intercalation Compounds (GIC) [75, 76]. The incorporation/conversion of F^- ions into the fluorocarbon matrix may be induced with an increase of the reaction temperature or the duration [73, 74].

The small amount of CF_2 and CF_3 groups in the case of pulsed fluorination shows that fluorination occurred without decomposition, therefore without the generation of defects, hereby confirming the Raman data. Indeed, the control of fluorination conditions avoids the hyperfluorination, and fluorine covalent grafting into the carbonaceous matrix occurs without the formation of important structural defects: the drastic control of the fluorination conditions

allows decreasing the number of structural defects such as CF_2, CF_3, and dangling bonds. These defects are always well correlated with the structural disorder [33, 42, 70].

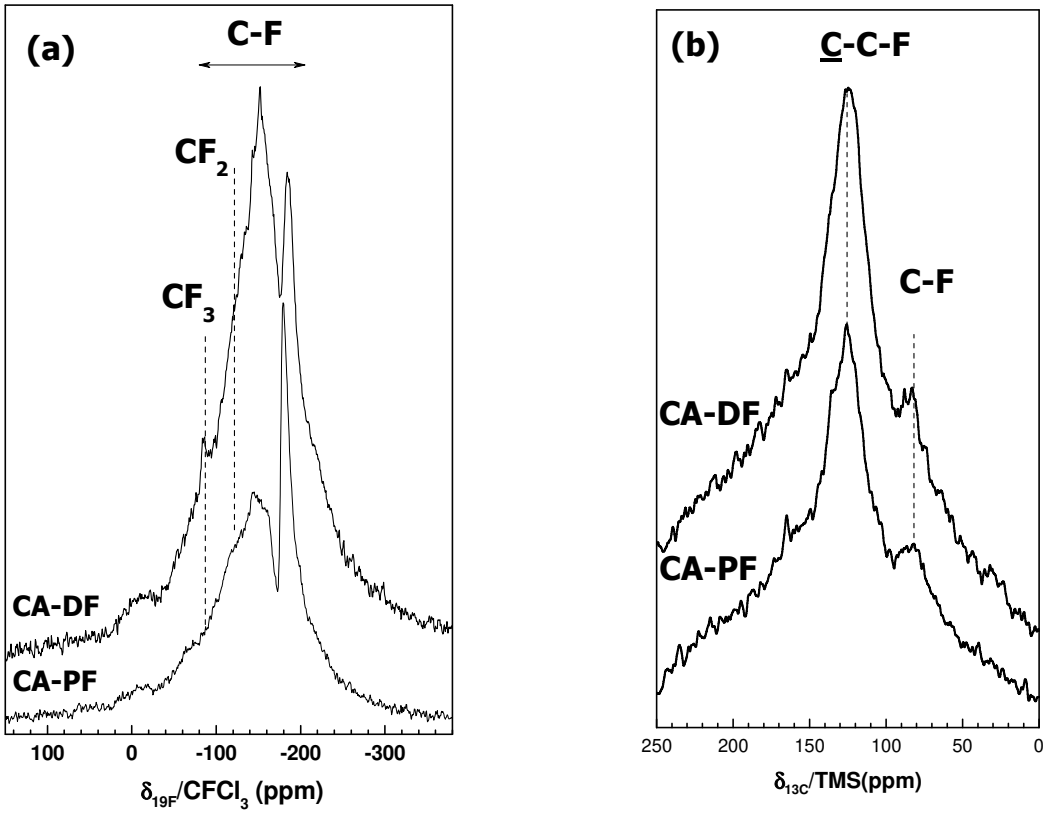

Figure 6. (a) ^{19}F and (b) ^{13}C MAS NMR spectra of CA-PF-$CF_{0.25}$ and CA-DF-$CF_{0.26}$ fluorinated aerogels with 34 and 10 kHz spinning rate, respectively.

Figure 6 shows the ^{13}C NMR spectra for CA –PF-$CF_{0.25}$ and CA-DF-$CF_{0.26}$. The mainline is observed at 125 ppm which is related to the non-fluorinated carbon (pure sp^2 hybridized carbons) without interaction with the fluorine atoms. The contribution at a chemical shift of 84 ppm is characteristic of a purely covalent C-F bond involving sp^3 hybridized carbon atoms and fluorine atoms. The relatively low intensity of this band is related to the low fluorine content in both samples.

An increasing fluorination rate decreases hyperconjugation (signifying weak interaction with neighboring C-F bonds) and strengthens the C-F covalent bond. Besides, the higher the fluorination, the greater the proportion of CF_2 groups [70, 77]; these groups give rise to a band at 110 ppm, not visible in our case, which confirms the low rate of defects generated by our fluorination methods, in agreement with Raman and ^{19}F NMR.

However, taking into account the low fluorination level and in agreement with Raman spectroscopy that did not indicate any change of structure of the CA, we consider that the fluorination mechanism that occurred was limited to the surface of the aerogels without

altering the bulk. NMR remains a useful tool for determining the level of volumetric fluorine content, though, as was shown elsewhere [34, 69, 78]. As a result, because of its conductive character, non-fluorinated areas (i.e. carbon) are mainly highlighted on the ^{13}C NMR spectra of those samples which explain the important peak at 125 ppm. Here the limits of the NMR method are reached due to the perturbation of the conduction electrons.

Again, because the CA used in this work have very low organization degrees (i.e. low graphitic character), no contribution at 42 ppm on ^{13}C spectra is observed, as opposed to other types of carbon such as carbon nanofibres CNF with a high graphitic degree [29, 34, 79, 80].

3.5 X-ray photoelectron spectroscopy (XPS)

To gain further information on the chemical composition of PF sample and to validate the low amount of CF_2 and CF_3 groups for pulsed fluorination, XPS was used as a fine probe for the determination of carbon bonding at the CA surface. Before fluorination (Figure a-b), the pristine carbon aerogel exhibits a main contribution at binding energy (BE) of 284.3 eV and a lower contribution at 285.6 eV ascribed to C-C bond and C-O bonds, respectively. Three other very weak contributions can be distinguished at BI of 287.2 eV, 288.8 eV and 290.4 eV corresponding to C=O, O-C=O and π- π* bonds, respectively. The relative abundances of carbon (95%) and oxygen (5%) are consistent with a weak oxidation of CA surface. After pulsed fluorination, (Figure c-e), the C-C (284.3 eV) and C-O (285.6 eV) contributions remain rather stable, and the component at 288.8 eV clearly increases due to the creation of C-F bonds [81-83]. Two weak contributions are detected at upper binding energies, corresponding to CHF-CHF bonds at 289.2 eV and to a higher carbon fluorination rate superimposed to the π- π* bonds (290.4 eV). These results are consistent with the F1s peak decomposition, which exhibits a main component at 686.4 eV and a weak contribution at 688.0 eV; these are ascribed to C-F and C-F2 bonds, respectively [81-83]. The relative abundances calculated after fluorination reveal that the fluorine contribution is around 13% whereas the amount of oxygen remains stable (6%).

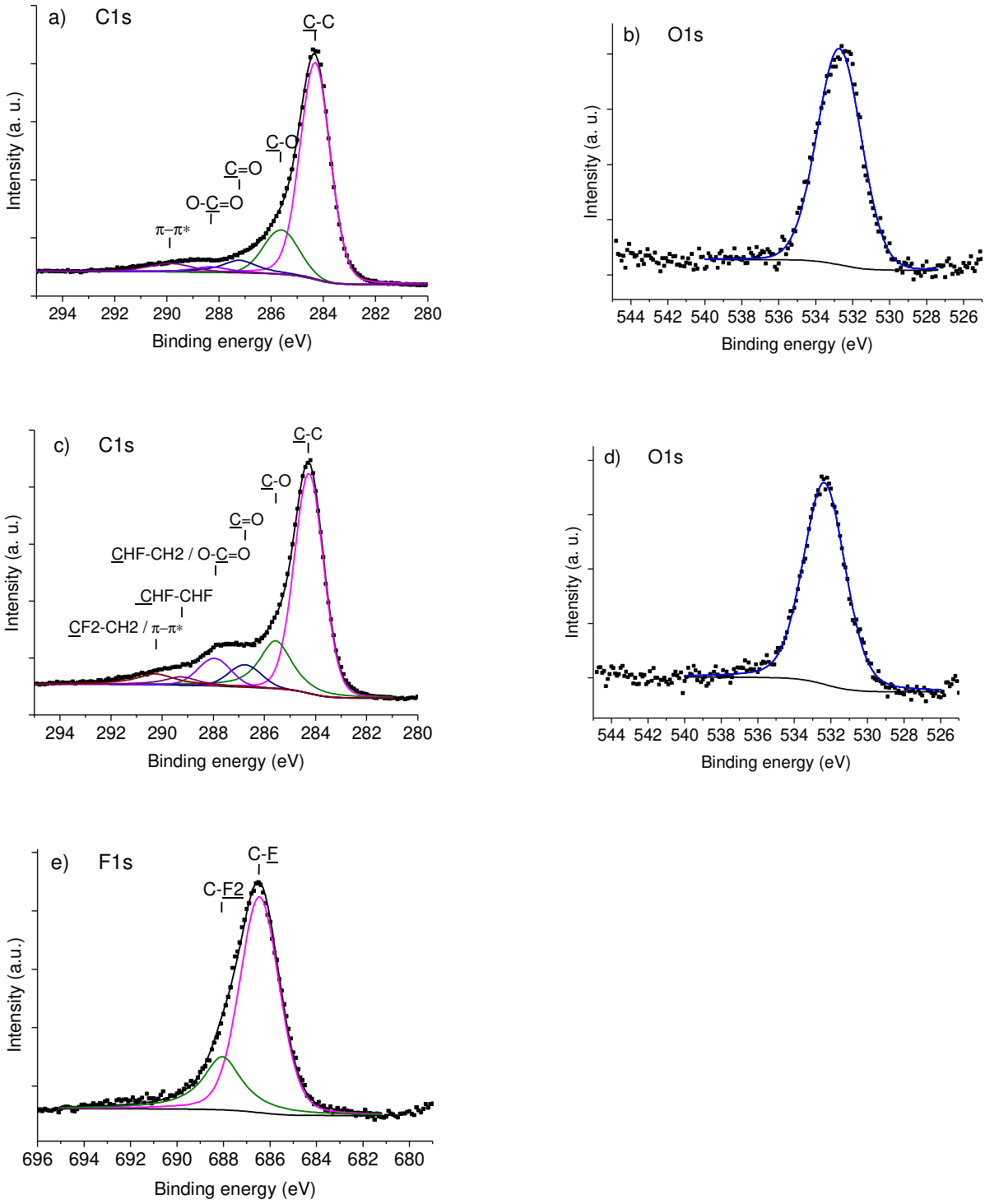

Figure 7. XPS spectra of pristine CA (a-b) and after (c-e) pulsed fluorination

Table 2. Estimated F/C ratio by weight uptake and XPS

Sample	%C	%O	%F	F/C (Δm)	F/C (XPS)
CA	**95**	**5**	**0**	-	-
CA-PF-CF$_{0.25}$	**81**	**6**	**13**	0.25	0.16

An extensive literature review of XPS studies of fluorinated carbons and XPS investigation of some reference compounds was carried out in order to explain the present XPS results. Nanse et al. [16] reviewed extensively the X-ray photoelectron spectroscopy for fluorocarbons. In these compounds, the binding energies of covalently bound C and F depend on the type of C concerned and on the structure to which these belong. At low temperature (T < 200-300°C), fluorine binds covalently to some surface C atoms (external surface, border of mesopores) and C of the subsuperficial zone of the carbon material; the possible components are : quaternary sp^3 C and sp^3 C of (-CH,-), (>CH-) groups or (-CH,-)$_n$, sequences bridging polyaromatic structural units, sp^3 C of cycles or saturated C chains linked to defects, gaps or discontinuities of the graphitic structure and which belong to the carbon skeleton of the starting material, functionalized (oxygenated or nitrogenated) sp^3 C and sp^2 C, sp^2 C of cycles of the border of the graphene layers, of non-conjugated aromatic cycles and non-aromatic unsaturated C. The sp^2 C of the graphene layers are not concerned, with the exception of those of the first atomic layer.

Thus, a fluorinated surface layer is formed, in which the amount of C atoms bound to F is clearly less important than in fluorinated graphite. The structure of the carbon skeleton of the starting material being largely preserved, in particular in non-fluorinated zones, the planar conformation of the graphene layers is not affected. The percentage of the superficial fluorinated carbon atoms (i.e. the amount of fluorine fixed by covalent binding at low temperature) is the more important when the starting material presents a lower degree of order (low degree of graphitization), which is the case for the carbon aerogels used in this work.

To summarize, the complete set of physico-chemical characterizations performed herein agree: the fluorinated CA are homogeneously and superficially fluorinated: no noticeable bulk structural and textural changes of the pristine CA structure are witnessed. As such, the present method of pulsed fluorination is compatible with a tight control of the fluorination, even for high surface area and poorly graphitized carbon structures.

3.6 Water trapping through thermal properties

Figure displays the TGA curves for the pristine and fluorinated aerogels with the same F/C ratio obtained by pulsed and direct fluorination. Table 3 summarizes the key values to evaluate thermal stability, namely T_{10} and $T_{C–F}$. Whatever the fluorination rate, the TGA curves may exhibit two-weight losses assigned to the de-fluorination at lower temperatures and oxidation of non-fluorinated carbon atoms with oxygen from the air (burning) at a higher temperature.

Comparing the TGA curves of pristine CA and the other fluorinated aerogels (Figure 8), fluorination seems to prevent water retention in the aerogel thanks to the hydrophobic character of the CFx created by the presence of fluorine atoms on the surface. Also, once fluorinated, the oxidation temperature of the non-fluorinated carbon (i.e. T_C) is shifted towards high values compared to pristine (Table 3). For instance, T_C for the pristine CA is 506°C, while that of the fluorinated samples, i.e. CA-PF-$CF_{0.25}$ and CA-DF-$CF_{0.26}$, are T_C = 534°C and 532°C, respectively.

Comparing the fluorinated samples, they both exhibit almost the same T_{C-F} and T_C values. However, their TGA curves indicate that the pulsed fluorination (CA-PF-$CF_{0.25}$) leads to a better hydrophobic character compared to the direct one (CA-DF-$CF_{0.26}$), although both materials have the same F/C ratio. Indeed, the weight drop (of about 10%) at 100°C related to the evaporation of the water initially adsorbed on the sample (see arrow on Figure 8) indicates smaller water retention for the for CA-PF-$CF_{0.25}$ sample and this is due to the different fluorination mechanisms in the pulsed fluorination; PF leads to more homogeneous repartition of fluorine atoms on the surface of the sample compared to the direct fluorination (see physicochemical characterizations in the previous sections). It's to note that the arrow on Figure 8 is only eye guide. The differences are observed in the 50-150°C range; because of the high specific surface area of the carbons, two adsorbed species may be released: water molecules and HF for fluorinated carbons. The thermal post-treatment at 150°C for 2 hours under primary vacuum removes HF, as well the weakest C-F bonds and adsorbed molecules like F_2, HF, NF_3, and C_2F_6. The data unambiguously evidence the benefit of the pulsed fluorination to avoid water re-adsorption after fluorination, i.e. the hydrophobic character.

The more homogeneous surface fluorination enabled by the PF versus the DF can be explained by a shorter exposure time to F_2 as well as the smaller quantities of fluorine used in the case of the pulsed method, resulting in a C-F repartition limited to the surface of the CA

material; an insulating and hydrophobic surface is created that limits the water retention inside the porosity of the CAs. That leads us to suppose that, for the dynamic process, the fluorination conditions (reaction time and F_2 available in sufficient abundance) lead to the incorporation of fluorine into the carbon matrix and to detrimental bulk fluorination.

In summary, DF leads to deep penetration of fluorine into the CA (bulk fluorination), whereas the depth of fluorination can be tightly controlled for the PF (i.e. surface fluorination).

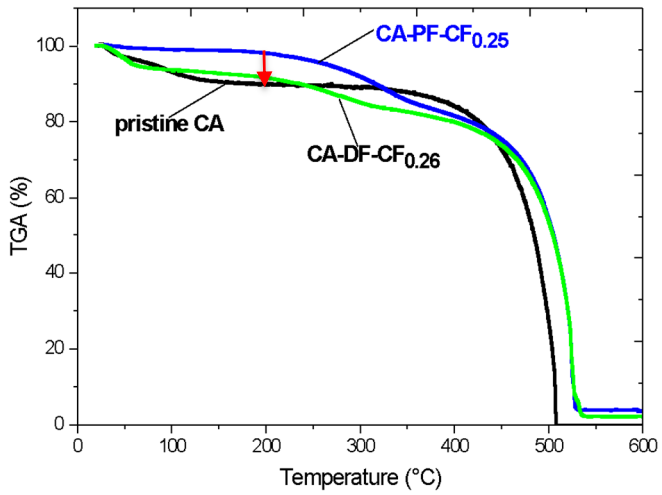

Figure 8. TGA curves for pristine and fluorinated aerogels. The arrow on the figure shows that water retention is lower for CA-PF-$CF_{0.25}$ compared to CA-DF-$CF_{0.26}$

Table 3. Key parameters deduced from TGA curves.

Sample	$T_{C\text{-}F}$ ± 2°C	T_C ±5°C
Pristine CA	--	506
CA-DF-$CF_{0.26}$	336	532
CA-PF-$CF_{0.25}$	339	534

To sum up this section, the traditional (direct) fluorination does not have a significant effect on the water retention and hence on the hydrophobicity. In fact, when the specific surface area is high, the reactivity towards F_2 increases; C-C bond cleavage may occur as it does for polymer, also very reactive [84, 85]. Some radicals (dangling bonds DB) are formed and reacted with fluorine while the other, a minority, remained on the treated sample. DB could also combine with oxygenated species during the treatment or during exposure to air. This latter process results in polar groups which increase the affinity for water molecule. The

reactive species F_2 were always in excess on the surface and the atmosphere was continuously renewed for the case of conventional dynamic process. It means also that those admixtures (mainly oxygen) in gaseous fluorine (less than 0.1 vol%) were also renewed and might react with DB. On the contrary, a few amounts of those admixtures were consumed in the closed reactor (static conditions for pulsed process), also by reaction with DB.

As indicated in the previous section, pulsed fluorination enables to obtain a fluorinated CA with interesting intrinsic properties regarding thermal and structural properties as well as the possibility of tailoring the water content within the porosity of the material. Also, the PF scored more benefits than the DF, especially in terms of a lower synthesis cost, thanks to the perfect control of the fluorination conditions (amount of F_2 used and reduced reaction time) this method offers, much better than DF. On the contrary, considering that PF is still in the conceptual stage contrary to the dynamic method which has a long and successful history, we decided to investigate further the sample obtained by pulsed fluorination, i.e. CA-PF-$CF_{0.25}$ using XPS analysis and conductivity measurements. Furthermore, in addition to its fundamental advantages, PF should be easily transferred to the industrial scale thanks to its ability to synthesize a larger amount of fluorinated carbons with lower cost compared to the dynamic one.

Finally as carbon aerogel are mainly used as electrode material, it was important to measure the conductivity of the CA after fluorination, as fluorination is known to confer an insulating character to its mother material.

3.7 Conductivity measurements

The value of the electrical conductivity depends primarily on the measurement method, but also on the materials' density and granulometry, the pressure applied, the temperature used, and the mass of the material tested. In this work, the electrical conductivities were measured at different pressures (0 or $6.37.10^7$ Pa) by applying 3 different intensities (-105 mA, 105 mA, and 400 mA). The resulting conductivities obtained with the different currents are close, indicating the homogeneity of each sample and a purely ohmic behavior. The average values are given in Table 4.

The electrical conductivity increases with the increase of the pressure applied but the tendency is the same whatever the pressure. The value of the pristine carbon aerogel is measured to be 2.27 S cm^{-1} ($6.37.10^7$ Pa) and 1.98 S cm^{-1} (0 Pa) which agrees with the value obtain for a carbon aerogel with a such density (0.15 g cm^{-3}) [86]. Fluorination at F/C = 0.25 decreases the conductivity down to 0.08 S.cm^{-1} which confirms a homogeneous fluorination

of the carbon surface. These conductivity values agree with those obtained by Asset et al. [55] and are an equivalent of a pristine CA with a density around 0.07 g cm^{-3} [86]. However, even if the conductivity is decreased through fluorination, this value is still acceptable owing to carbon nanostructures application which requires a high level of conductivity on the range of 20–100 S m^{-1} while retaining the structural integrity [87].

Table 4. Electrical conductivity values for pristine and fluorinated samples at different applied pressures

sample	**Fluorination at. ratio F/C**	**σ_e average ($S.m^{-1}$)**	**σ_e average ($S.m^{-1}$)**
	±0.02	**$6.37x10^7$ Pa (±5)**	**0 Pa (±5)**
CA	0	198	227
CA-PF-$CF_{0.25}$	0.25	5	8

Conclusion

Carbon aerogels (CAs) are an important type of porous carbons that may find applications in many domains including energy storage and conversion, catalysis, adsorption and sorbents, and desalination. The utility of CA is derived from their high surface area, three-dimensional open structure, chemical stability, the abundance of carbon, and their low mass density. However, CA usually suffer from water trapping into their porosity, which can severely handicap the intended process. To address this issue, CAs were fluorinated using two fluorination methods, both operating at room temperature and using molecular fluorine F_2. The main difference between the two fluorination methods resides in the injection of the exact amount of reactive fluorine via several controlled pulsed injections (pulsed fluorination, PF), and under a continuous F_2 flow i.e an excess of fluorine for the dynamic fluorination (DF). Pulsed fluorination offers an advantage over the direct method in terms of i) elaborating a homogeneous distribution of fluorine at the carbon surface, ii) tailoring the water content of the CA and results in more hydrophobic materials that enables to limit water retention**.** In addition, the ability to i) enhance thermal and chemical stabilities without drastic structural changes and to control the electrical conductivity by pulsed fluorination enhances the potential utility of this class of CAs. New applications of porous carbon aerogels will likely

be developed in the near term thanks to the treatment by fluorination. These applications in which the novel properties of fluorinated CAs will make them uniquely suited.

Acknowledgments

The authors would like to thank the French National Research Agency program (ANR-14-CE05-0047 project CORECAT) for the funding. We also thank Ms. Elodie Petit, M. Fabien Labbé and Ms. Charlotte Gervillié for their valuable contribution in this work.

References

[1] A. Stein, Z. Wang, M.A. Fierke, Functionalization of Porous Carbon Materials with Designed Pore Architecture, Adv. Mater. 21(3) (2009) 265-293.
[2] Y.-S. Hu, P. Adelhelm, B.M. Smarsly, S. Hore, M. Antonietti, J. Maier, Synthesis of Hierarchically Porous Carbon Monoliths with Highly Ordered Microstructure and Their Application in Rechargeable Lithium Batteries with High-Rate Capability, Adv. Funct. Mater. 17(12) (2007) 1873-1878.
[3] J. Chmiola, G. Yushin, Y. Gogotsi, C. Portet, P. Simon, P.L. Taberna, Anomalous Increase in Carbon Capacitance at Pore Sizes Less Than 1 Nanometer, Science 313(5794) (2006) 1760-1763.
[4] S. Tabata, H. Iida, T. Horie, S. Yamada, Hierarchical porous carbon from cell assemblies of rice husk for in vivo applications, Med. Chem. Comm 1(2) (2010) 136-138.
[5] K.T. Lee, J.C. Lytle, N.S. Ergang, S.M. Oh, A. Stein, Synthesis and Rate Performance of Monolithic Macroporous Carbon Electrodes for Lithium-Ion Secondary Batteries, Adv. Funct. Mater. 15(4) (2005) 547-556.
[6] G.S. Chai, I.S. Shin, J.-S. Yu, Synthesis of Ordered, Uniform, Macroporous Carbons with Mesoporous Walls Templated by Aggregates of Polystyrene Spheres and Silica Particles for Use as Catalyst Supports in Direct Methanol Fuel Cells, Adv. Mater. 16(22) (2004) 2057-2061.
[7] T.J.B.b. John K. Brennan, Kendall T. Thomson c, Keith E. Gubbins Water in porous carbons, Colloids Surface A. 187-188 (2001) 539–568.
[8] F. Schüth, K.S.W. Sing, J. Weitkamp, Handbook of porous solids, Wiley-VCH, Weinheim, Germany, 2002.
[9] W.T. Tsai, C.Y. Chang, Surface chemistry of activated carbons and its relevance for effects of relative humidity on adsorption of chlorinated organic vapors, Chemosphere 29(12) (1994) 2507-2515.
[10] P.G. V. Bourdin, A. Malka-Edery., Fundamentals of Adsorption; Proceedings of the Sixth Conference on Fundamentals of Adsorption, presqu'ile de Giens, France, 24–26 May 1998, Elsevier, Paris, 1998, p. 1167.
[11] M. Pouzet, M. Dubois, K. Charlet, A. Béakou, From hydrophilic to hydrophobic wood using direct fluorination: A localized treatment, Comptes Rendus Chimie 21(8) (2018) 800-807.
[12] Y. Ahmad, N. Batisse, M. Dubois, K. Guérin, F. Labbé, R. Metkemeijer, S. Berthon-Fabry, B. Molina Concha, F. Maillard, L. Dubau, R. Chattot, M. Chatenet, Fluorination of carbon based electrocatalysts for enhanced durability of PEMFC, SFEC Colloque de la Société Francophone d'Etude des Carbones, Carqueiranne, France, 2016.
[13] W. Zhang, M. Dubois, K. Guerin, P. Bonnet, H. Kharbache, F. Masin, A.P. Kharitonov, A. Hamwi, Effect of curvature on C-F bonding in fluorinated carbons: from fullerene and derivatives to graphite, Phys. Chem. Chem. Phys. 12(6) (2010) 1388-1398.
[14] H. Touhara, J. Inahara, T. Mizuno, Y. Yokoyama, S. Okanao, K. Yanagiuch, I. Mukopadhyay, S. Kawasaki, F. Okino, H. Shirai, W.H. Xu, T. Kyotani, A. Tomita, Property control of new forms of carbon materials by fluorination, J. Fluorine Chem. 114(2) (2002) 181-188.
[15] Y. Tian, H. Yue, Z. Gong, Y. Yang, Enhanced electrochemical performance of fluorinated carbon nanotube as cathode for Li–O2 primary batteries, Electrochim. Acta 90(0) (2013) 186-193.
[16] G. Nansé, E. Papirer, P. Fioux, F. Moguet, A. Tressaud, Fluorination of carbon blacks. An X-ray photoelectron spectroscopy study. Part II. XPS study of a furnace carbon black treated with gaseous fluorine at temperatures below 100 °C. Influence of the reaction

parameters and of the activation of the carbon black on the fluorine fixation, Carbon 35(3) (1997) 371-388.
[17] A. Tressaud, T. Shirasaki, G. Nansé, E. Papirer, Fluorinated carbon blacks: influence of the morphology of the starting material on the fluorination mechanism, Carbon 40(2) (2002) 217-220.
[18] J. Marie, R. Chenitz, M. Chatenet, S. Berthon-Fabry, N. Cornet, P. Achard, Highly porous PEM fuel cell cathodes based on low density carbon aerogels as Pt-support: Experimental study of the mass-transport losses, J. Power Sources 190(2) (2009) 423-434.
[19] M. Ouattara-Brigaudet, S. Berthon-Fabry, C. Beauger, M. Chatenet, N. Job, M. Sennour, P. Achard, Influence of the carbon texture of platinum/carbon aerogel electrocatalysts on their behavior in a proton exchange membrane fuel cell cathode, Int. J. Hydrog. Energy 37(12) (2012) 9742-9757.
[20] L. Castanheira, L. Dubau, M. Mermoux, G. Berthomé, N. Caqué, E. Rossinot, M. Chatenet, F. Maillard, Carbon Corrosion in Proton-Exchange Membrane Fuel Cells: From Model Experiments to Real-Life Operation in Membrane Electrode Assemblies, ACS Catal. 4(7) (2014) 2258-2267.
[21] L. Castanheira, W.O. Silva, F.H.B. Lima, A. Crisci, L. Dubau, F. Maillard, Carbon Corrosion in Proton-Exchange Membrane Fuel Cells: Effect of the Carbon Structure, the Degradation Protocol, and the Gas Atmosphere, ACS Catal. 5(4) (2015) 2184-2194.
[22] F. Labbé, E. Disa, Y. Ahmad, K. Guérin, T. Asset, F. Maillard, M. Chatenet, R. Metkemeijer, S. Berthon-Fabry, Tin dioxide coated carbon materials as an alternative catalyst support for PEMFCs: Impacts of the intrinsic carbon properties and the synthesis parameters on the coating characteristics, Micropor. Mesopor. Mat. 271 (2018) 1-15.
[23] S. Berthon-Fabry, L. Dubau, Y. Ahmad, K. Guerin, M. Chatenet, First Insight into Fluorinated Pt/Carbon Aerogels as More Corrosion-Resistant Electrocatalysts for Proton Exchange Membrane Fuel Cell Cathodes, Electrocatalysis 6(6) (2015) 521-533.
[24] Tressaud A, Moguet F, Flandrois S, Chambon M, Guimon C, Nansé G, Papirer E, Gupta V, Bahi OP, On the nature of C--F bonds in various fluorinated carbon materials : XPS and TEM inverstigation, J. Phys. Chem. Solid 57(6-8) (1996) 745-51.
[25] A. Tressaud, E. Durand, C. Labrugère, Surface modification of several carbon-based materials: comparison between CF4 rf plasma and direct F2-gas fluorination routes,J. Fluorine Chem. 125(11) (2004) 1639-1648.
[26] A. Tressaud, E. Durand, C. Labrugère, A.P. Kharitonov, L.N. Kharitonova, Modification of surface properties of carbon-based and polymeric materials through fluorination routes: From fundamental research to industrial applications,J. Fluorine Chem. 128(4) (2007) 378-391.
[27] S. Zhou, S.D. Sherpa, D.W. Hess, A. Bongiorno, Chemical Bonding of Partially Fluorinated Graphene, J.Phys. Chem. C 118(45) (2014) 26402-26408.
[28] P.F. Fulvio, S.S. Brown, J. Adcock, R.T. Mayes, B. Guo, X.-G. Sun, S.M. Mahurin, G.M. Veith, S. Dai, Low-Temperature Fluorination of Soft-Templated Mesoporous Carbons for a High-Power Lithium/Carbon Fluoride Battery, Chem.Mater. 23(20) (2011) 4420-4427.
[29] F. Chamssedine, M. Dubois, K. Guérin, J. Giraudet, F. Masin, D.A. Ivanov, L. Vidal, R. Yazami, A. Hamwi, Reactivity of Carbon Nanofibers with Fluorine Gas, Chem. Mater. 19(2) (2006) 161-172.
[30] M. Dubois, K. Guerin, W. Zhang, Y. Ahmad, A. Hamwi, Z. Fawal, H. Kharbache, F. Masin, Tuning the discharge potential of fluorinated carbon used as electrode in primary lithium battery, Electrochim. Acta 59 (2012) 485-491.
[31] K. Guérin, J.P. Pinheiro, M. Dubois, Z. Fawal, F. Masin, R. Yazami, A. Hamwi, Synthesis and characterization of highly fluorinated graphite containing sp2 and sp3 carbon, Chem.Mater. 16(9) (2004) 1786-1792.
[32] K. Guérin, M. Dubois, A. Houdayer, A. Hamwi, Applicative performances of fluorinated carbons through fluorination routes: A review,J. Fluorine Chem. 134(0) (2012) 11-17.

[33] Y. Ahmad, E. Disa, M. Dubois, K. Guérin, V. Dubois, W. Zhang, P. Bonnet, F. Masin, L. Vidal, D.A. Ivanov, A. Hamwi, The synthesis of multilayer graphene materials by the fluorination of carbon nanodiscs/nanocones, Carbon 50(10) (2012) 3897-3908.
[34] Y. Ahmad, K. Guérin, M. Dubois, W. Zhang, A. Hamwi, Enhanced performances in primary lithium batteries of fluorinated carbon nanofibers through static fluorination, Electrochim. Acta 114(0) (2013) 142-151.
[35] N. Batisse, K. Guérin, M. Dubois, A. Hamwi, L. Spinelle, E. Tomasella, Fluorination of silicon carbide thin films using pure F2 gas or XeF2, Thin Solid Films 518(23) (2010) 6746-6751.
[36] F. Chamssedine, K. Guérin, M. Dubois, E. Disa, E. Petit, Z.E. Fawal, A. Hamwi, Fluorination of single walled carbon nanotubes at low temperature: Towards the reversible fluorine storage into carbon nanotubes, J. Fluorine Chem. 132(12) (2011) 1072-1078.
[37] Dubois M. , Guérin K., Giraudet J., Pilichowski J.F., Thomas P. , Delbé K., Mansot J.L. , Hamwi A., Direct fluorination of poly(p-phenylene), Polym. J. 46(18) (2005) 6736-45.
[38] M. Murakami, K. Matsumoto, R. Hagiwara, Y. Matsuo, 13C/19F high-resolution solid-state NMR studies on layered carbon-fluorine compounds, Carbon 138 (2018) 179-187.
[39] W. Feng, P. Long, Y. Feng, Y. Li, Two-Dimensional Fluorinated Graphene: Synthesis, Structures, Properties and Applications, Adv. Sci. 3(7) (2016) 1500413.
[40] J. Kim, R. Zhou, K. Murakoshi, S. Yasuda, Advantage of semi-ionic bonding in fluorine-doped carbon materials for the oxygen evolution reaction in alkaline media, RSC Adv. 8(26) (2018) 14152-14156.
[41] M. Dubois, K. Guérin, Y. Ahmad, N. Batisse, M. Mar, L. Frezet, W. Hourani, J.-L. Bubendorff, J. Parmentier, S. Hajjar-Garreau, L. Simon, Thermal exfoliation of fluorinated graphite, Carbon 77 (2014) 688-704.
[42] M. Dubois, K. Guérin, J.P. Pinheiro, Z. Fawal, F. Masin, A. Hamwi, NMR and EPR studies of room temperature highly fluorinated graphite heat-treated under fluorine atmosphere, Carbon 42(10) (2004) 1931-1940.
[43] A.F. Maxwell, J.S. Fry, L.A. Bigelow, The Indirect Fluorination of Cyanuric Chloride1, J.Am.Chem. Soc. 80(3) (1958) 548-549.
[44] N.S. Chilingarov, J.V. Rau, L.N. Sidorov, L. Bencze, A. Popovic, V.F. Sukhoverkhov, Atomic fluorine in thermal reactions involving solid TbF4, J Fluorine Chem. 104(2) (2000) 291-295.
[45] J.K. Gibson, R.G. Haire, Thermal decomposition of curium tetrafluoride and terbium tetrafluoride, J Solid State Chem. 73(2) (1988) 524-530.
[46] W. Zhang, K. Guérin, M. Dubois, Z.E. Fawal, D.A. Ivanov, L. Vidal, A. Hamwi, Carbon nanofibres fluorinated using TbF4 as fluorinating agent. Part I: Structural properties, Carbon 46(7) (2008) 1010-1016.
[47] Y. Ahmad, M. Dubois, K. Guérin, A. Hamwi, W. Zhang, Pushing the theoretical limit of Li–CFx batteries using fluorinated nanostructured carbon nanodiscs, Carbon 94 (2015) 1061-1070.
[48] T. Fuchigami, S. Inagi, Electrochemical Fluorination for Preparation of Alkyl Fluorides, in: J. Hu, T. Umemoto (Eds.), Fluorination, Springer Singapore, Singapore, 2017, pp. 1-22.
[49] V.P. Reddy, HF Fluorination for the Synthesis of Alkyl Fluorides, in: J. Hu, T. Umemoto (Eds.), Fluorination, Springer Singapore, Singapore, 2017, pp. 1-14.
[50] P. Lam, R. Yazami, Physical characteristics and rate performance of (CFx)n ($0.33<x<0.66$) in lithium batteries, J. Power Sources 153(2) (2006) 354-359.
[51] G. Nagasubramanian, B. Sanchez, A new chemical approach to improving discharge capacity of Li/(CFx)n cells, J. Power Sources 165(2) (2007) 630-634.
[52] F. Labbé, Y. Ahmad, K. Guérin, B. Molina Concha, M. Chatenet, R. Metkemeijer, S. Berthon-Fabry, Carbon aerogels coated with tin dioxide as catalyst supports for proton exchange membrane fuel cells, 3rd International Seminar on Aerogels 2016 : “Properties-Manufacture-Applications”, Sophia Antipolis, France, 2016.

[53] F. Labbé, T. Asset, M. Chatenet, Y. Ahmad, K. Guérin, R. Metkemeijer, S. Berthon-Fabry, Activity and Durability of Platinum-Based Electrocatalysts with Tin Oxide–Coated Carbon Aerogel Materials as Catalyst Supports, Electrocatalysis 10(2) (2019) 156-172.
[54] Y. Ahmad, K. Guérin, L. Dubau, M. Chatenet, S. Berthon-Fabry, Proton Exchange Membrane Fuel Cell With Enhanced Durability Using Fluorinated Carbon As Electrocatalyst, E3S Web of Conferences 16 (2017) 17001.
[55] T. Asset, R. Chattot, F. Maillard, L. Dubau, Y. Ahmad, N. Batisse, M. Dubois, K. Guérin, F. Labbé, R. Metkemeijer, S. Berthon-Fabry, M. Chatenet, Activity and Durability of Platinum-Based Electrocatalysts Supported on Bare or Fluorinated Nanostructured Carbon Substrates, J. Electrochem. Soc. 165(6) (2018) 3346-3358.
[56] W. Zhang, K. Guérin, M. Dubois, A. Houdayer, F. Masin, A. Hamwi, Carbon nanofibres fluorinated using TbF4 as fluorinating agent. Part II: Adsorption and electrochemical properties, Carbon 46(7) (2008) 1017-1024.
[57] Pekala R.W., Organic aerogels from the polycondensation of resorcinol with formaldehyde, Journal of Material Science 24(9) (1989) 3221-27.
[58] M. Dubois, K. Guérin, Y. Ahmad, N. Batisse, M. Mar, L. Frezet, W. Hourani, J.-L. Bubendorff, J. Parmentier, S. Hajjar-Garreau, L. Simon, Thermal exfoliation of fluorinated graphite, Carbon 77 (2014) 688-704.
[59] E. Disa, M. Dubois, K. Guérin, H. Kharbache, F. Masin, A. Hamwi, The effect of nanostructure on the thermal properties of fluorinated carbon nanofibres, Carbon 49(14) (2011) 4801-4811.
[60] W. Zhang, L. Moch, M. Dubois, Gu, K. rin, J. Giraudet, me, F. Masin, A. Hamwi, Direct Fluorination of Carbon Nanocones and Nanodiscs, J.Nanosci. Nanotechnol. 9(7) (2009) 4496-4501.
[61] A. Jablonski, Evaluation of procedures for overlayer thickness determination from XPS intensities, Surf. Sci.688 (2019) 14-24.
[62] M.A. Mahjoub, G. Monier, C. Robert-Goumet, L. Bideux, B. Gruzza, New method for the determination of the correction function of a hemisperical electron analyser based on elastic electron images, J.Electron Spectrosc.197 (2014) 80-87.
[63] L.G. Cançado, K. Takai, T. Enoki, M. Endo, Y.A. Kim, H. Mizusaki, A. Jorio, L.N. Coelho, R. Magalhães-Paniago, M.A. Pimenta, General equation for the determination of the crystallite size La of nanographite by Raman spectroscopy, Appl. Phys. Lett. 88(16) (2006) 163106.
[64] Z. Wang, X. Huang, R. Xue, L. Chen, Dispersion effects of Raman lines in carbons, J.Appl. Phys. 84(1) (1998) 227-231.
[65] J.D. Roberts, F.J. Weigert, Carbon-13 nuclear magnetic resonance spectroscopy. Determination of carbon-fluorine couplings, J.Am.Chem. Soc. 93(10) (1971) 2361-2369.
[66] S.L. Manatt, M.A. Cooper, C.W. Mallory, F.B. Mallory, Evidence for a steric effect on directly bonded carbon-fluorine and carbon-proton nuclear magnetic resonance couplings, J.Am.Chem. Soc. 95(3) (1973) 975-977.
[67] E.W. Della, E. Cotsaris, P.T. Hine, Synthesis and carbon-13 nuclear magnetic resonance studies of some bridgehead fluorides: carbon-fluorine coupling constants, J.Am.Chem. Soc. 103(14) (1981) 4131-4135.
[68] Nakajima T., Watanabe N., Graphite Fluorides and Carbon–Fluorine Compounds Boca Raton Ann Arbor Boston: CRC Press, Boston, (1991).
[69] W. Zhang, M. Dubois, K. Guérin, A. Hamwi, J. Giraudet, F. Masin, Solid-state NMR and EPR study of fluorinated carbon nanofibers, J. Solid State Chem. 181(8) (2008) 1915-1924.
[70] J. Giraudet, M. Dubois, K. Guérin, C. Delabarre, A. Hamwi, F. Masin, Solid-State NMR Study of the Post-Fluorination of (C2.5F)n Fluorine–GIC, J.Phys.Chem. B 111(51) (2007) 14143-14151.
[71] Y. Sato, K. Itoh, R. Hagiwara, T. Fukunaga, Y. Ito, On the so-called “semi-ionic” C–F bond character in fluorine–GIC, Carbon 42(15) (2004) 3243-3249.

[72] F. Leroux, M. Dubois, Origin of the highly enhanced porosity of styryl LDH hybrid-type carbon replicas and study of a subsequent fluorination at low-temperature, J.Mater.Chem. 16(46) (2006) 4510-4520.
[73] C. Matei Ghimbeu, K. Guerin, M. Dubois, S. Hajjar-Garreau, C. Vix-Guterl, Insights on the reactivity of ordered porous carbons exposed to different fluorinating agents and conditions, Carbon 84 (2015) 567-583.
[74] J. Parmentier, S. Schlienger, M. Dubois, E. Disa, F. Masin, T.A. Centeno, Structural/textural properties and water reactivity of fluorinated activated carbons, Carbon 50(14) (2012) 5135-5147.
[75] Panich AM, Nuclear magnetic resonance study of fluorine–graphite intercalation compounds and graphite fluorides, Synth. Metals 100(2) (1999) 169-185.
[76] F.Y. Fujiwara, J.S. Martin, Heterobihalide ions. Nuclear magnetic resonance spectroscopy of strong hydrogen bonds, J.Am.Chem. Soc. 96(25) (1974) 7625-7631.
[77] Giraudet J, Dubois M, Guérin K, Pinheiro JP, Hamwi A, Stone WEE, Pirotte P, Masin F. , Solid-state F-19 and C-13 NMR of room temperature fluorinated graphite and samples thermally treated under fluorine: Low-field and high-resolution studies, J. Solid State Chem. 178 (2005) 1262-1268.
[78] Y. Ahmad, M. Dubois, K. Guerin, A. Hamwi, E. Flahaut, High energy density of primary lithium batteries working with sub-fluorinated few walled carbon nanotubes cathode, J. Alloys Compd. 726 (2017) 852-859.
[79] E. Jeong, M.-J. Jung, Y.-S. Lee, Role of fluorination in improvement of the electrochemical properties of activated carbon nanofiber electrodes,J. Fluorine Chem. 150(0) (2013) 98-103.
[80] R. Yazami, A. Hamwi, K. Guérin, Y. Ozawa, M. Dubois, J. Giraudet, F. Masin, Fluorinated carbon nanofibres for high energy and high power densities primary lithium batteries, Electrochem. Comm 9 (2007) 1850-1855.
[81] V.G. Nazarov, Structure and composition of the surface layer in polymers modified by elemental fluorine, J.Appl.Polym.Sci. 95(4) (2005) 897-902.
[82] G. Nansé, E. Papirer, P. Fioux, F. Moguet, A. Tressaud, Fluorination of carbon blacks: An X-ray photoelectron spectroscopy study: III. Fluorination of different carbon blacks with gaseous fluorine at temperatures below 100 °C influence of the morphology, structure and physico-chemical characteristics of the carbon black on the fluorine fixation, Carbon 35(4) (1997) 515-528.
[83] J. Zha, S.S. Ali, J. Peyroux, N. Batisse, D. Claves, M. Dubois, A.P. Kharitonov, G. Monier, T. Darmanin, F. Guittard, L.N. Alekseiko, Superhydrophobicity of polymer films via fluorine atoms covalent attachment and surface nano-texturing, J. Fluorine Chem. 200 (2017) 123-132.
[84] A.P. Kharitonov, G.V. Simbirtseva, V.M. Bouznik, M.G. Chepezubov, M. Dubois, K. Guérin, A. Hamwi, H. Kharbache, F. Masin, Modification of ultra-high-molecular weight polyethylene by various fluorinating routes, J. Polym. Sci. Pol. Chem. 49(16) (2011) 3559-3573.
[85] A.P. Kharitonov, Direct fluorination of polymers—From fundamental research to industrial applications, Prog. Org. Coat.61(2) (2008) 192-204.
[86] X. Lu, O. Nilsson, J. Fricke, R.W. Pekala, Thermal and electrical conductivity of monolithic carbon aerogels, J.Appl. Phys. 73(2) (1993) 581-584.
[87] A. Tevlek, A.M.N. Atya, M. Almemar, M. Duman, D. Gokcen, A.Y. Ganin, H.H.P. Yiu, H.M. Aydin, Synthesis of Conductive Carbon Aerogels Decorated with β-Tricalcium Phosphate Nanocrystallites, Sci.Rep. 10(1) (2020) 5758.